JOURNAL OF AIRCRAFT
Vol. 37, No. 3, May–June 2000

Wind-Tunnel Tests of an Aircraft Turret Model

C. H. Snyder* and M. E. Franke†
Air Force Institute of Technology, Wright–Patterson Air Force Base, Ohio 45433
and
M. L. Masquelier‡
U.S. Air Force Research Laboratory, Wright–Patterson Air Force Base, Ohio 45433

The drag of a half-scale aircraft laser turret is investigated in a low-speed wind tunnel. Forces, moments, and pressures are recorded for the turret and aft-mounted fairings and splitter plates. Oil traces and tufts indicate that the flow is characterized by dominant vortices shedding from the top of the turret and a large trailing wake of vorticity. Splitter plates are ineffective in reducing drag as a result of the strong flow over the top of the turret. A small fairing reduces the baseline drag coefficient by 49% but is unable to produce attached flow near the turret. A large fairing eliminates nearly all separation regions and reduces the baseline drag coefficient by 55%.

Nomenclature

C_D = drag coefficient, D/qS
C_n = yaw-moment coefficient
C_p = pressure coefficient, $(P - P_{\text{atm}})/q$
C_y = side-force coefficient
D = drag force
P = pressure
q = dynamic pressure, $\frac{1}{2}\rho V^2$
Re_D = Reynolds number (based on diameter)
S = frontal area of turret
V = wind-tunnel velocity
x = positive out turret leading edge
y = positive according to right-hand rule
z = positive toward turret base
β = sideslip angle
ρ = density

Introduction

TURRETS have been placed on aircraft for many applications. There is recent interest in placing a turret on an aircraft for purposes of laser communications research. Without some method of streamlining, the turret's shape could induce a significant drag penalty. In addition, regions of separated flow near the turret surface can degrade the laser's optical signal or produce vibrations that adversely affect the tracking system.

Significant research has been dedicated to producing efficient means of reducing drag on shapes such as cylinders and spheres.[1] The turret considered in this study is mainly spherical in shape, but blended to a cylindrical base near the point of attachment to the aircraft. In this configuration, existing cylindrical or spherical drag results offer little in the form of good drag predictions. However, drag results of similar shapes or configurations could prove extremely valuable, but tests on turret shapes have been limited, and such results are difficult to locate.

Several tests of similar turret shapes were carried out in the mid-1970s in support of the Airborne Laser Laboratory (ALL) program. Emphasis was placed on minimizing the drag, aerodynamic forces, and vibrations placed on a turret with an open viewing port.[2] Many methods of drag reduction were tested, including fore and aft fairings, side fairings, boundary-layer suction, mass-flow injection, and scoops and channels placed near the top of the turret. One test determined the lowest drag configuration to consist of the turret, forward ramped shell, and aft fairing, which decreased the drag by 30% compared to the lone turret configuration.[3]

Key differences between earlier configurations and the turret tested in this study made predictions based on previous results difficult. Laser technology has advanced to the level of using a window over the viewing area that matches the curvature of the turret itself. Also, previous turrets were tested on a cylindrical surface approximating the fuselage of a large transport aircraft; this study considered a turret to be mounted on the flat underside of an aircraft. Finally, more stringent operational limits have been placed on the size of any modifications added to the testbed aircraft, and the laser window must have an unobstructed view (field of regard) of certain areas around the turret. Thus, any drag reduction modifications limited by the laser's field of regard (look angles) may not be ideal from an aerodynamic drag standpoint.

This study investigated the low-speed aerodynamics of a turret model by measuring forces, moments, and pressures acting on the turret. The objective was to characterize the flowfield around the turret, identify regions of separation, and investigate the use of passive aft-mounted drag-reduction devices (splitter plates and fairings) while meeting the field-of-regard requirements of the laser. An important tradeoff for any modifications to the actual turret was the field of regard (look angles) available to the laser system compared with the improvement in drag. Splitter plates offered the least look-angle restrictions whereas the fairings produced larger restrictions.

The investigation did not model the characteristics of the overall flowfield of an aircraft; rather, the tests were designed to characterize the relative differences in drag and local flowfield associated with the installation of the splitter plates and fairings on the turret model. The turret model was a half-scale model of a proposed turret. The frontal area of the model was approximately 0.05 m^2 (0.5 ft^2) compared with the proposed full-scale turret frontal area of approximately 0.19 m^2 (2 ft^2). The drag coefficient was referenced to the frontal area of the turret model.

When examining stability properties, each drag-reduction configuration was tested at sideslip angles of 5 deg and smaller. Results in this area did not represent the full range of sideslip angles encountered in flight, but the model structure and wind-tunnel safety concerns limited this phase of testing to small angles. In normal operation, the aircraft will rarely exceed a 3-deg sideslip, and so the sideslip range was considered adequate.

Presented as paper 99-0939 at the AIAA 37th Aerospace Sciences Meeting and Exhibit, Reno, NV, 11–14 January 1999; received 8 June 1999; revision received 3 February 2000; accepted for publication 8 February 2000.

*1st Lieutenant, U.S. Air Force; currently U.S. Air Force Research Laboratory, Wright–Patterson Air Force Base, OH.
†Professor, Department of Aeronautics and Astronautics. Associate Fellow AIAA.
‡Senior Technical Staff, Sensors Directorate. Senior Member AIAA.

Fig. 1 Laser turret model.

Experimental Apparatus

Tests were conducted in the Air Force Institute of Technology (AFIT) 1.5-m- (5-ft-) diam low-speed wind tunnel at a 0-deg angle of attack and freestream velocities up to 65 m/s (213 fps). Reynolds numbers ranged from 3×10^5 to 9×10^5 based on the turret diameter. The size of the AFIT 1.5-m (5-ft) wind tunnel allowed for testing and flow visualization of a half-scale model. The dynamic pressure in the test section (tunnel q) was determined from the difference between the total pressure of the flow (atmospheric) and the static pressure measured at the inlet to the test section. The desired flow velocity, calculated directly from the dynamic pressure, was obtained by varying the coarse and fine speed controls of the fan motors.

The turret model shown in Fig. 1 was a half-scale model of a proposed aircraft turret for housing laser optics. Created from a large block of laminated mahogany, the turret model was a 0.23-m- (9.25-in.-) diam sphere blended to a 0.2-m- (8-in.-) diam cylindrical base. Installed in the spherical portion of the turret using 0.1-cm (0.040-in.) outer diameter stainless steel tubing were 11 static pressure taps. Six taps were aligned with the vertical plane, beginning with the stagnation point in front and running over the top of the turret in 30-deg intervals. Five taps were placed in the horizontal plane around the diameter of the sphere, beginning 90 deg aft of the stagnation point and continuing rearward in 15-deg intervals. A large cylindrical cutout within the model provided for the routing of pressure-tap tubing.

Two splitter plates with different heights were tested for drag reduction and are shown in Fig. 2. Both splitter plates were 0.48-cm- ($\frac{3}{16}$-in.-) thick aluminum, 2.6 turret diameters in length, allowing an unobstructed look angle in the horizontal plane of nearly 150 deg measured from the front stagnation point. The splitter plate thickness near the turret was 0.95 cm ($\frac{3}{8}$ in.) thick to allow for the mounting bolts. The plates were bolted to the turret model, supported by two braces, and cantilevered 0.95 cm ($\frac{3}{8}$ in.) above the ground plane to ensure they would not contact the ground plane and invalidate the force data.

Shown in Fig. 3, the small and large blended fairings tested for drag reduction were manufactured from a synthetic mahogany material to provide higher strength than mahogany and an added safety factor. The interiors of the fairings were hollowed to reduce weight, leaving shells with an average 1.6-cm ($\frac{5}{8}$-in.) wall thickness. The small and large fairings allowed unobstructed 120- and 90-deg look angles, respectively. Both fairings were the same length, were

Fig. 2 Splitter plates.

Fig. 3 Fairings.

cantilevered the same distance above the ground plane, and shared the same attachment points to the turret as the splitter plates.

A rectangular wood platform (ground plane) spanned the test section and was securely fastened in the test section to simulate a predominantly flat aircraft underside and provide a mounting system for the model and its instrumentation. An elliptical leading edge reduced the turbulence created as the flow split above and below the ground plane. Forces and moments were measured only on the turret and its various configurations and did not include the ground plane.

A 0.32-m- (12.5-in.-) diam cavity hole for instrumentation was located 1.17 m (46 in.) aft of the ground plane leading edge and centered between the left and right sides of the ground plane. The instrumentation cavity, essentially an aluminum inverted top hat, served as a mounting platform for the load cell unit (LCU), which, in turn, was centered within the cavity and attached to the turret model. Instrumentation wires and tubes connected to the model ran through a hole in the cavity wall to the data acquisition systems in the wind-tunnel control room. An aluminum cover ring placed flush with the surface of the ground plane surrounded the base of the turret model and covered the exposed portions of the instrumentation cavity (Fig. 1). A 0.48-cm ($\frac{3}{16}$-in.) gap between the ring and the turret allowed deflection of the turret during testing.

The LCU was used to determine the three forces and three moments acting on the turret under each configuration. Eight load cells were arranged to give symmetric loading in each direction. Each load cell had a sensitivity of ±0.08 mm (0.003 in.) over the load cell range of 111 N (25 lbf). The theory of the LCU and the details of its calibration and use are given by King.[4]

All data were acquired with a graphical-software package for data acquisition installed on a personal computer. The LCU signals were

processed through signal conditioners (with a gain of 50), which provided a clean and steady excitation voltage to the LCU. The signal conditioners were connected to a data acquisition board, at which point the signal was converted from analog to digital. An interface card was installed in the personal computer and connected to the data acquisition board to give the software access to the digital signals.

A microcomputer-based, stand-alone pressure measurement system was used to measure the static pressure at various locations on the turret surface. The static taps were connected to an electronic pressure scanner placed in the cavity beneath the model. Signals from the pressure scanner passed to an analog-to-digital converter and into the pressure-system processor. The personal computer accessed the pressure-system processor via the interface card. Snyder[5] gives further details of the instrumentation.

Experimental Procedures and Data Reduction

Calibrations

The LCU was calibrated manually with known weights to determine the eight individual load-cell responses (voltages). Forces and moments were isolated into each of the primary directions while the turret was placed in precisely the same configuration as during testing. Any stiffness of the wires and tubes within the turret assembly was minimized by placing slack in all wires and connecting the stainless-steel, pressure-tap tubing to flexible Tygon tubing.

The calibrations in each positive and negative direction produced lines with slopes nearly identical in magnitude for the primary load cells. The slopes of the linear calibration curves were calculated from a least-squares fit to the data and placed into a coefficient matrix. All primary calibration curves had a correlation coefficient of at least 0.9999. During the testing phase, the forces and moments acting on the model were calculated by multiplying the measured voltage vector by the inverse of the coefficient matrix. A MATLAB® routine reduced the raw data files into the various force and pressure coefficients.

A test-section blockage factor was applied to adjust for all objects placed in the test section. Using Rae and Pope's correlation,[6] the combined area of the ground plane, instrumentation cavity, and turret model gave a blockage correction of 0.0148. Thus, the measured wind-tunnel velocity was corrected by multiplying by 1.0148. The drag coefficient for the turret was referenced to the turret frontal area, 0.045 m^2 (0.485 ft^2) based on a computer drawing of the full-scale turret.

A set of commands directed the pressure-measurement system to perform a self-calibration at the beginning of each set of runs. Once started, the stand-alone pressure system would apply a series of known pressures to the electronic pressure scanner and isolate each pressure tap in turn. The result was a set of calibration curves that was used to calculate the pressures in the 11 static taps on subsequent runs.

Testing

Five separate configurations were tested during this study: clean turret, small or large splitter plate attached, and small or large fairing attached. For each of the four latter configurations, data were taken at 0-, ±2.5-, and ±5-deg sideslip angles, but the clean turret was tested at 0 deg each time. When the model was rotated, the LCU rotated as well, so that all data were taken with respect to the model coordinate axes. The tunnel velocity ranged from 20 m/s (66 ft/s) to 65 m/s (213 ft/s). The maximum speed tested corresponded to a Mach number of 0.19.

The forces and pressures acting on the model were zeroed before beginning each data run and checked at the end of each run to catch any shift in data, but no hysteresis effects were encountered during testing. At each tunnel speed, 2000 samples were taken from the LCU and static-pressure system at a scan rate of 2024 samples per second. The samples were then averaged into one data point and saved. Before changing the tunnel speed, 10 such data points were taken.

Flow Visualization

Tufts

The turret, both fairings, and the small splitter plate were extensively tufted for this phase of the study. Embroidery thread (of several contrasting colors) 0.8 mm ($\frac{1}{32}$ in.) thick was cut into 1.3-cm ($\frac{1}{2}$-in.) lengths and placed on the model in a closely spaced grid pattern. Tufts of this size were useful in identifying separation regions, the strength of separated flow, and dominant flow frequencies. The tufts did induce a small amount of flowfield interference. A lack of optimal viewing windows on one side of the tunnel dictated that tufts be placed predominantly on the opposite side of the model. Several tufts were placed on the poor visibility side of the model to ensure flow symmetry, but these tufts were not photographed. Each tuft was applied using a triangular piece of fiber tape. A drop of quick-drying glue placed onto the free end of each tuft prevented fraying when the tufts were subjected to the rapid unsteady motions of the flow in the wind tunnel.

Still photographs and high-speed video were taken of the various tufted configurations. The still photographs covered the overall configuration with slight emphasis on the area near the junction of the turret and the fairing/splitter plate. The high-speed video segments were recorded at 200 frames per second and provided views of the entire tufted area as well as separate close-ups of the junction.

Oil Flow

Oil flows were used to identify the surface flows around the clean turret and the effects of the gap above the instrumentation cavity. Prior to this phase, the turret and surrounding area on the ground plane were painted flat black to give the greatest contrast to the white oil. A blend of Rosco Fluid (used in fog makers) and titanium dioxide (for white pigment) was applied to the turret in hundreds of tiny flecks by snapping the bristles of a small brush held several inches from the turret. While the turret was still wet, the tunnel speed was brought up to 55 m/s (180 ft/s) and the drops were spread in the direction of the flow around the turret. When a steady-state condition was reached, the tunnel was turned off and pictures were taken of the oil streamlines on the turret. This method yielded sharp, descriptive flow images and has traditionally been shown to yield very good information about the flow on a body surface.[7]

Results and Discussion

Quantitative data collected in this study consisted of forces and pressures acting on the turret model with and without the fairings or splitter plates attached. These data were used to quantify the changes in drag, pressure distribution, and stability characteristics with the addition of each drag-reduction device. Flow visualization provided further explanation for the reasons why these changes were taking place.

Flowfield Description

Clean Turret

The flowfield at the front of the unmodified (clean) turret is illustrated in Fig. 4 by oil flow that was produced at 55 m/s (180 ft/s) for a duration of approximately 1 min. The larger stationary oil drops in Fig. 4 indicate the stagnation region at the front of the turret, whereas the miniscule stationary oil drops scattered over the entire turret surface simply did not contain sufficient oil to allow motion along the surface. The oil streaks that originated at the edges of the stagnation region indicate the direction of the flow as it was forced over and around the turret. A small amount of reverse (upstream) flow can be seen on the ground plane near the front of the turret, and the remaining flow on the ground plane was directed around and away from the base of the turret.

The flow near the base of the turret can be visualized as a horseshoe vortex that forms at the front of the turret and extends around the sides and far downstream, similar to the horseshoe vortex described by Belik[8] that develops near the junction between a body and a wall.

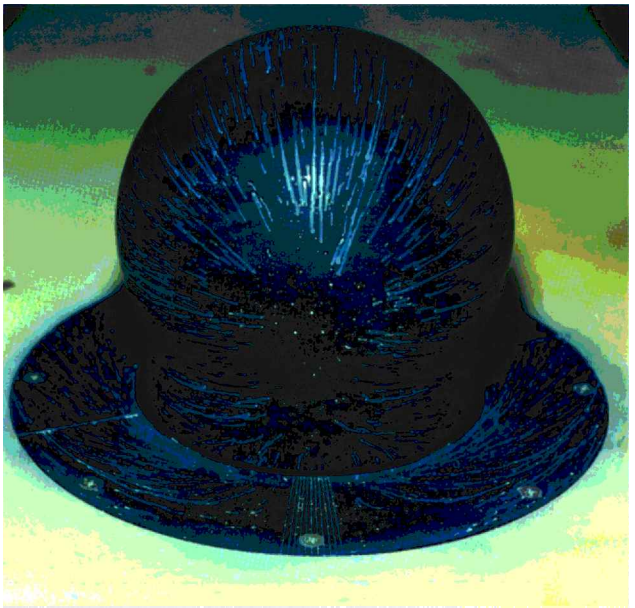

Fig. 4 Oil flow, front view of turret.

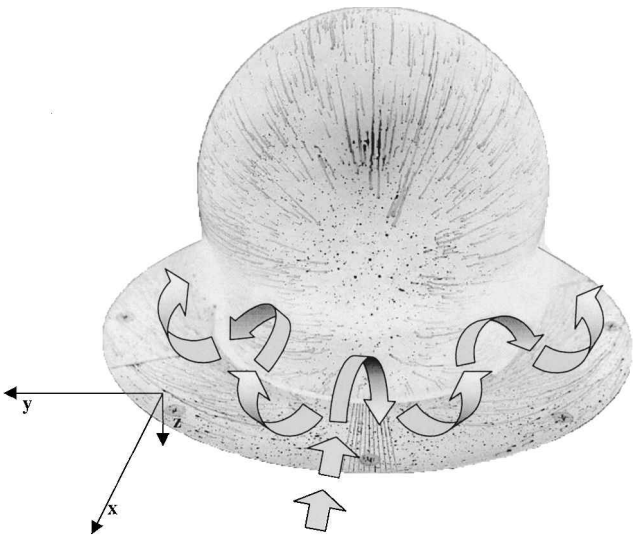

Fig. 5 Horseshoe vortex representation.

Figure 5 shows that as the flow approached the area on the turret where the spherical portion was blended to the cylindrical base, the flow was turned downward and began to form a vortex rotating about the *y* axis. A combination of the turret geometry and the velocity profile in the boundary layer of the ground plane (high velocity at the upper edge of the boundary layer and zero velocity at the ground plane) caused the flow to begin its downward rotation. Viewed over time, this process generated a vortex near the base of the turret rotating about the *y* axis.

The Blasius solution predicted a turbulent boundary-layer thickness of 1.9 cm (0.75 in.) at the front of the turret, and this was approximately the height at which downward flow appeared on the turret in Figs. 4 and 5. The developing vortex then wrapped around the sides of the turret while continuing to rotate as shown. The direction of rotation caused a stagnation region on the turret near the top of the vortex and an upward velocity component above the vortex. There was also stagnated flow in small separated regions on the ground plane and turret base beginning at approximately 90 deg from the front of the turret.

The main separation zone occurred at the rear of the turret as shown by the oil flow in Fig. 6. The oil flow also captured the reverse flow on the ground plane in the wake of the turret. Although the oil flow seems to indicate a well-behaved separation bubble behind the

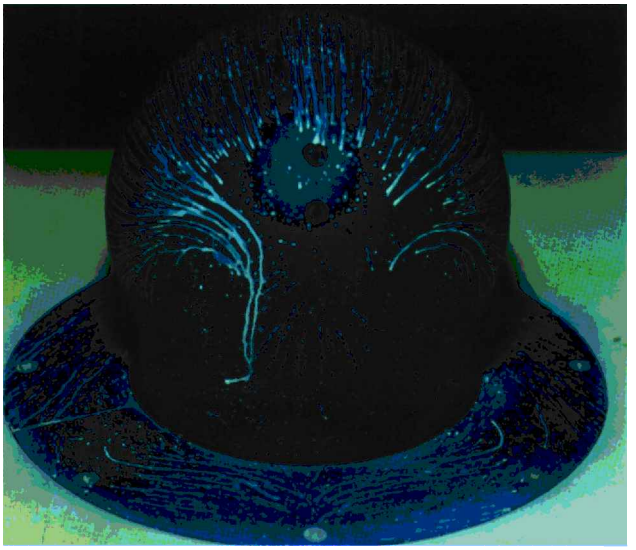

Fig. 6 Oil flow, rear view of turret.

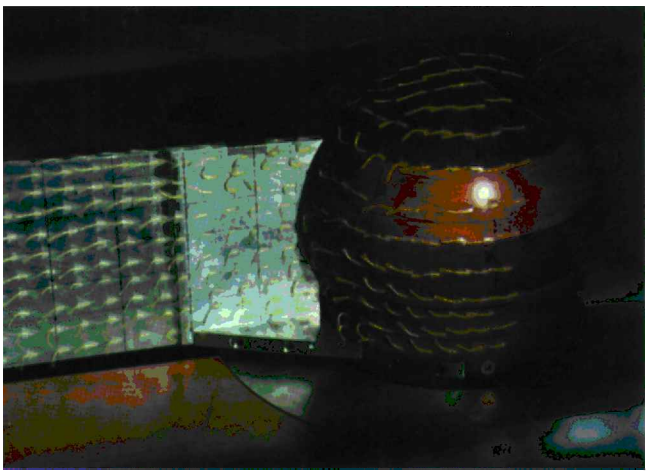

Fig. 7 Tuft run, small splitter plate installed.

turret, high-speed video of the tufts and qualitative tuft-on-a-wire tests portrayed a highly chaotic and turbulent region. In addition to the vortex street shed from the sides of the turret (similar to those encountered behind a circular cylinder), high-intensity vortices were shed from the top of the turret. Gravity acting on a large quantity of oil in the separation zone caused the large vertical streaks to appear in Fig. 6; these should not be regarded as an indication of the flow in that region. Tuft observations indicated separation near 125 deg (within ±5 deg), which is 10–15 deg forward of the point where the oil flow stopped.

The photographs and high-speed video of the tufts gave dynamic descriptions of the flow near the surface of the turret. The flow remained attached through approximately 120 deg aft of the leading edge. Rapidly oscillating tufts near and beyond the 125-deg meridian appeared blurred in the photographs indicating that the flow had become separated. Tufts along the top of the turret showed separation near 125 deg from the front as well. High-speed video indicated that tufts in the separated region generally oscillated between frequencies of 20–50 Hz. Near the base of the turret, the tufts captured the upward motion of the flow above the horseshoe vortex.

Splitter Plates

Tuft photographs taken of the turret with the small splitter plate indicated the splitter plate did not alter the 125-deg separation point on the turret by any noticeable amount (Fig. 7). The splitter plate did reduce the motion of the vortex street in the wake of the turret; however, the tuft motion on the turret itself closely resembled that

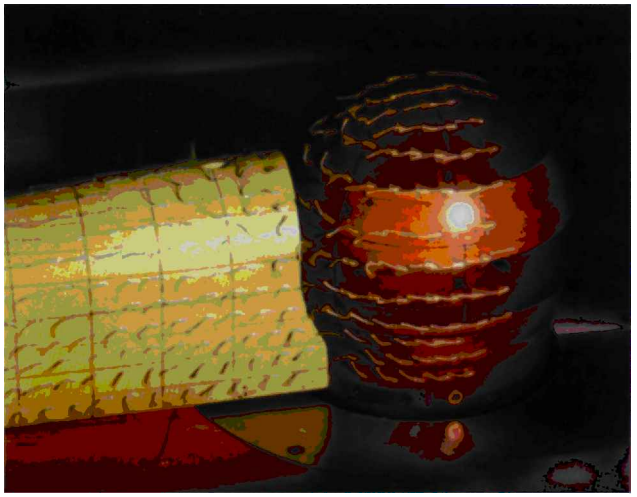

Fig. 8 Tuft run, small fairing installed.

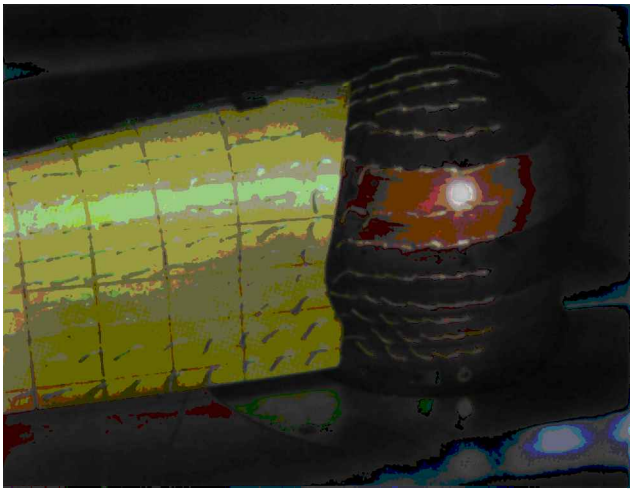

Fig. 9 Tuft run, large fairing installed.

seen on the clean turret. At the base of the turret, three tufts bent completely backward demonstrated strong reverse flow near the ground plane. The tufts on the upstream portion of the splitter plate were in a strong separation zone and were turned sharply upwards or downwards depending on their position on the splitter plate. Because the splitter plate reduced the strength of the vortices shed from the sides of the turret, the flow over the top of the turret became increasingly dominant and easier to visualize.

Figure 7 is the strongest indication of the dominant top vortices that were shed from the top of the turret and rotated about the *y* axis, much like the initial rotation of the horseshoe vortex. Although only partially shown in Fig. 7, the tufts indicated a consistent downward motion for one diameter aft of the splitter plate/turret junction. The remaining tufts did not show a dominant flow direction but simply oscillated about horizontal lines drawn on the splitter plate. This verified that the splitter plate did not prevent separation; it was able to reduce the motion of the vortices shed from the sides of the turret but could not prevent the dominant top vortices from developing behind the turret. The splitter plate was, therefore, ineffective in reducing the size of the low-pressure wake behind the turret.

Fairings

The flow around the turret with the small fairing installed is shown in Fig. 8. The most striking feature is the relatively large separation zone located upstream and downstream of the fairing attachment point. Although the small fairing provided a streamlined shape for the flow to attach onto behind the turret, the flow remained separated for approximately 1.3 diameters along the fairing. This occurred because the small fairing was located well within the separated wake of the turret. The large separated region near the fairing attachment point resulted in poor flow quality in that area. The tufts in that separated region gave an additional indication of the strong vortices shedding from the top of the turret. Near the top of the fairing, several rows of tufts showed strong reverse flow, whereas the tufts on the lower half of the fairing displayed a sharp downward flow velocity. Separation appeared along the top and sides of the turret (with small fairing attached) at approximately the same points as on the clean turret, 125 deg behind the leading edge.

With the large fairing, the separation region near the fairing attachment point was nearly eliminated, as shown in Fig. 9. Flow along the side of the turret showed slight separation near the last column of tufts placed on the turret (approximately 135 deg from the turret leading edge). This separation region was extremely small, however, and in most cases the flow reattached to the fairing within approximately 0.2 turret diameters. A region of downward velocity occurred near the fairing/turret junction and the base of the fairing, but this region was much smaller and weaker than that of the small fairing. The main reason for this vast improvement in flow quality of the large fairing over the small fairing was the reduction in strength of the vortices shed from the top of the turret. Figure 9 shows the height of the large fairing extending nearly to the top of the turret. Consequently, the flow over the top of the turret remained attached for the entire length of the turret and fairing. With the top flow completely attached and the side flow attached for all but approximately 0.2 diameters aft of the junction, the flowfield created by this configuration was extremely well behaved, and as will be shown, considerable drag savings resulted.

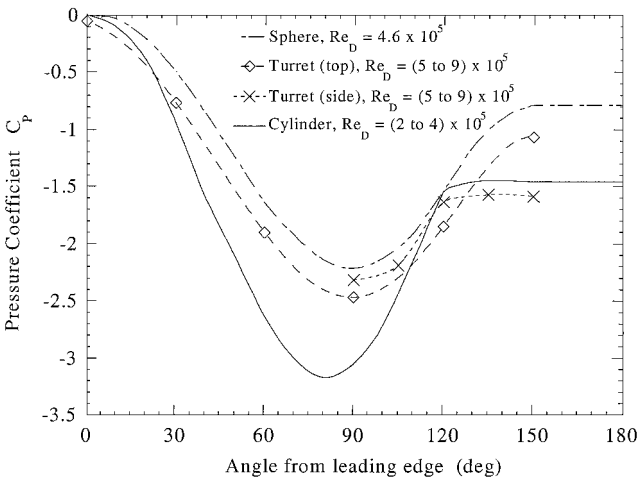

Fig. 10 Pressure distributions, similar shapes.

Pressure Distributions

Clean Turret

The pressure distributions along the top and sides of the clean turret are plotted in Fig. 10 against experimental distributions for a sphere and an infinite cylinder from previous studies.[1] Because the flow over the top of the turret encountered the same hemispherical shape as the flow over the top of a sphere, the turret and sphere pressure distributions have similar curves. With the base of the turret connected to the ground plane, however, the curves suggest a higher air velocity around the top and sides of the turret than that around the corresponding areas of a sphere at a given Reynolds number.

The pressure distribution around the side of the turret closely followed the sphere distribution in the range of 90–120 deg behind the front of the turret. Beyond 120 deg, however, the pressure distribution closely followed that of an infinite cylinder, becoming nearly constant and indicating flow had separated from the sides of the turret. The pressure distribution along the side also verified the visual estimation of separation at 125 deg from tuft and oil flow pictures. Along the top of the turret, a lack of pressure taps between 120 and 150 deg did not allow actual identification of the top separation point. It is highly probable the top separation point was in agreement with the flow-visualization observations.

Splitter Plates

The pressure distributions around the turret with the small splitter plate installed were similar to those around the clean turret (Fig. 10). The side separation point appeared to be slightly forward of 125 deg. The tuft photographs did not detect this difference because the change was within the ±5-deg error band inherent in the tuft measurements. The pressures along the top of the turret showed larger changes, however. From 90 deg aft of the leading edge and beyond, the pressures on the turret (with the splitter plate installed) were roughly 8% higher than the pressures on the clean turret. The pressures with the large splitter plate installed were approximately the same as those encountered with the small splitter plate.

Fairings

The pressure distributions around the turret with the small fairing installed are shown in Fig. 11. Similar to the splitter plates, the small fairing covered the last pressure tap along the top (150 deg). In addition, the fairing covered the last pressure tap along the side of the turret (150 deg). With the rear pressure tap covered by the fairing and no pressure taps in the fairing itself, a complete description of the increased pressure recovery behind the turret cannot be given. Unlike the splitter plates, though, the fairings produced a significant pressure recovery along both the top and side of the turret.

Figure 11 indicates that the small fairing delayed separation slightly along the side, whereas with the large fairing (not shown) separation did not even occur by 135 deg. The much smaller separation zone near the large fairing in Fig. 9 verifies delayed separation, but the tufts in Fig. 8 do not indicate any delayed separation with the small fairing attached. Because separation was delayed with the large fairing and the pressure data are significantly more accurate and quantitative than the tufts, it is likely that separation was delayed when the small fairing was installed.

Drag

Clean Turret

The measured drag coefficient for the clean turret is shown in Fig. 12 together with experimental data for related shapes from other studies.[1] Although the turret was partially a sphere, the turret drag coefficient was nearly four times higher than a sphere at a Reynolds number of 6×10^5 and higher. A sphere encounters pressure relief on all sides, and the resulting separation region does not begin until approximately 155 deg from the leading edge.[1] For the turret configuration, however, the separation and low-pressure region was much larger and resulted in a large increase in pressure drag.

Figure 12 also shows that the turret drag coefficient was quite similar to a finite cylinder with a diameter-to-height ratio of one placed perpendicularly on a flat plate (a very similar configuration to the turret). The turret's slightly lower drag coefficient can be attributed to the streamlining near the top of the turret that is not present in the finite cylinder. Unfortunately, data for the finite cylinder were taken at a Reynolds number of approximately 1×10^5 and cannot be accurately extrapolated to the Reynolds number range in which the turret was tested. Assuming the flow around the cylinder is still laminar at 1×10^5, the cylinder is likely to experience a similar drag decrease in the higher-Reynolds-number range of Fig. 12. When this occurs, drag decreases as the flow transitions from laminar to turbulent and remains attached to the cylinder for a greater distance around the circumference.

Splitter Plates

As predicted, the splitter plates were able to reduce the vortex strength around the sides of the turret and produce a small reduction in drag. At the higher velocities tested, Fig. 13 shows a 7% reduction in drag coefficient for the small splitter plate and a 5% reduction for the large splitter plate. With nearly identical pressure distributions around the top and side of the turret, it can be expected that the pressure recovery and pressure drag, respectively, for each splitter plate configuration would not be significantly different. Because the surface area of the large splitter plate was approximately 17% greater, though, the large splitter plate configuration incurred an additional amount of skin-friction drag.

The three-dimensional nature of the flow around the turret resulted in much poorer splitter plate performance than previous two-dimensional splitter plate studies have shown. For a cylinder spanning between two walls, a 4.2-diam-length splitter plate was able to reduce the drag by 43% at Reynolds numbers between 10^4 and 10^5. For the same cylinder, an extremely short splitter plate (known as a

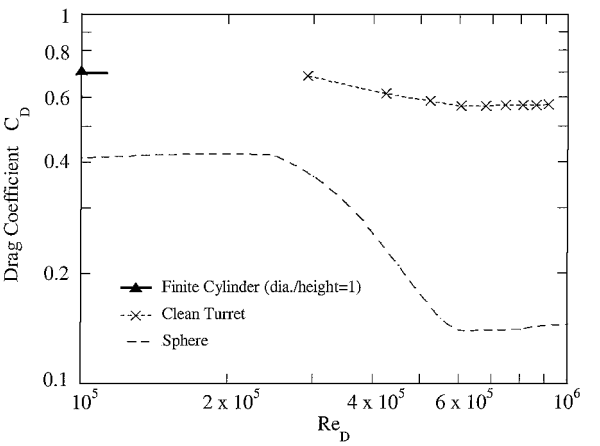

Fig. 12 Drag coefficients, similar shapes.

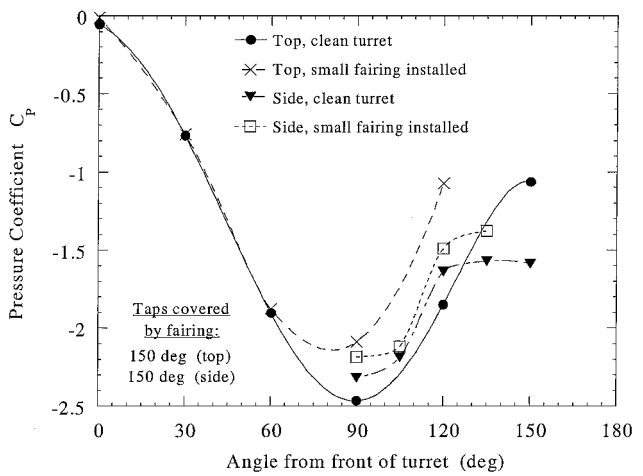

Fig. 11 Pressure distributions, small fairing.

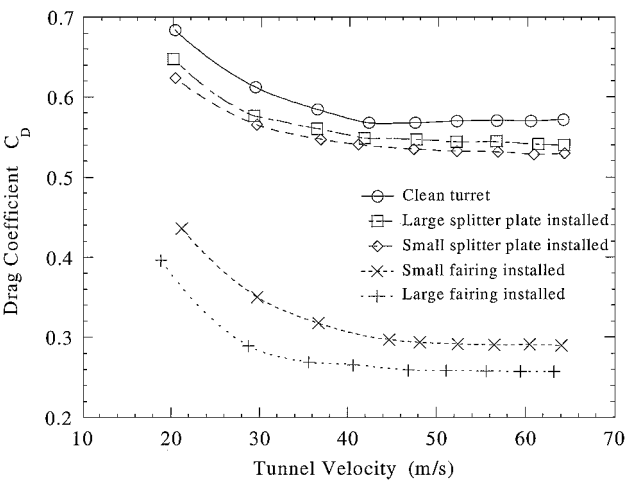

Fig. 13 Drag coefficients, fairings, and splitter plates.

Thwaites flap) extended only one-quarter of a diameter behind the cylinder but still reduced the drag by 15% (Ref. 1).

Fairings

The small and large fairings resulted in drag coefficient reductions of 49% and 55%, respectively, compared with the clean turret (Fig. 13). The streamlined shapes of the fairings reduced drag by delaying separation and allowing the flow to reattach behind the turret, thereby inducing a greater pressure recovery. Although the small fairing was too far within the separation region to eliminate the strong top vortices and cause significant reattachment, it was still able to achieve a drag reduction comparable to the large fairing by causing pressure recovery and preventing suction from acting on a portion of the turret. The greater success of the large fairing was a direct result of streamlining the top flow and creating attached flow over the vast majority of the turret/fairing surface. However, the larger surface area of the large fairing resulted in higher skin-friction drag than the small fairing, which partially reduced the large fairing's overall success in reducing drag. Tuft behavior suggested that the position of the fairings also broke up the large-scale vortices in the wake and forced smaller, less-powerful vortices to form behind the turret instead.

In a study on two-dimensional circular cylinders,[1] a wedge-shaped aft fairing with a 2.1-diameter length (placed along the entire span of the cylinder) produced a 39% drag reduction at a Reynolds number of approximately 3×10^5. The maximum thickness of the fairing was nearly the same as the cylinder diameter, but the simple wedge configuration was shorter and less streamlined than the large fairing/turret configuration in this study. This result highlights the success of using longer, more streamlined fairings even though the fairings were not as wide as the turret diameter. Even with three-dimensional effects, the fairings in this study created greater drag reductions than a two-dimensional wedge-shaped fairing as thick as the diameter of the cylinder it was placed behind.

The low-speed drag results from this study are of interest for low-speed flight of an aircraft with a turret installed. However, as airspeed is increased past the point where sonic flow appears at the sides of the turret, the clean-turret drag coefficient should show a sharp increase. This characteristic was documented in the wind-tunnel tests of the ALL turret, during which the wind-tunnel Mach number ranged from 0.6 to 0.9. At Mach 0.6, the clean-turret drag coefficient was approximately 0.65, and it increased to 1.1 at Mach 0.9 (Ref. 3). In comparison, a clean-turret drag coefficient of 0.56 at Mach 0.19 was found in this study (Fig. 13).

The critical Mach number for a sphere is 0.57, above which shocks begin to form at the sides of the sphere and drag increases sharply.[9] Thus, the flow around the ALL turret was most likely critical at Mach 0.6, which could explain the 16% higher drag coefficient measured for the ALL (at Mach 0.6) vs the drag coefficient for the turret model (at Mach 0.19). However, even at transonic airspeeds, a fairing placed behind the ALL turret was capable of reducing the baseline drag coefficient by 30%. This suggests that the fairings tested in this study would probably provide considerable drag reduction also at transonic speeds.

Stability Properties

The side-force coefficients for each of the four drag-reduction configurations are shown in Fig. 14. For each configuration, a rotation into the wind resulted in a force proportional to the angle of rotation. The constant of proportionality varied for each configuration; the larger or less streamlined shapes produced higher side-force coefficients at a given sideslip angle. Thus, the worst configuration (the one that produced the highest side forces) was the large splitter plate, followed by the small splitter plate, large fairing, and small fairing.

The nonlinear yaw-moment results were not quite as intuitive as those for the side-force coefficient, however. As the trailing edge of each fairing or splitter plate was rotated into the wind, the expected result was a restoring yaw moment that tended to weathervane the configuration parallel with the freestream. In stability terms, this would translate into a positive C_n vs β slope. The splitter plates had positive C_n vs β slopes, as expected, but the fairings had negative

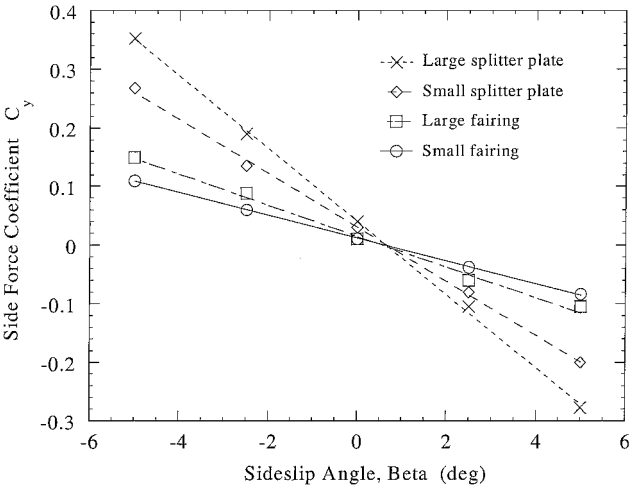

Fig. 14 Side-force coefficients.

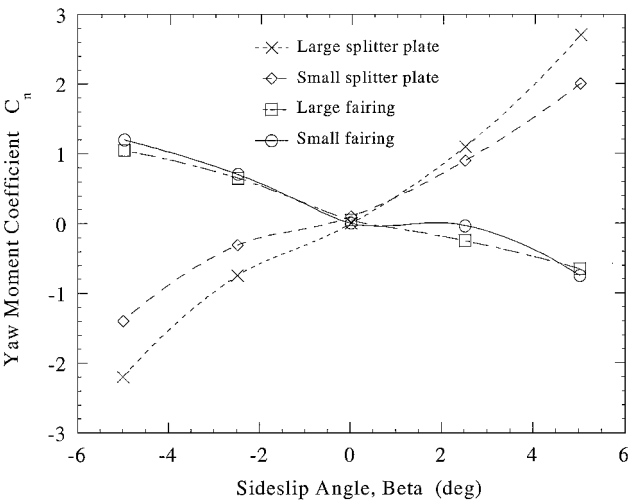

Fig. 15 Yaw-moment coefficients.

(destabilizing) C_n vs β slopes. Instead of aligning the fairing/turret configuration with the freestream, Fig. 15 indicates that both fairings tended to rotate further into the wind when placed at a sideslip angle up to ±5 deg. The stability data and tuft photographs collected during this part of the study suggest that the destabilizing moments occurred as a result of the small sideslip angles tested. The following discussion highlights a possible cause for this phenomenon, but additional testing is needed to verify this or any other such cause.

At sideslip angles of 5 deg and less, no portion of the fairings was visible beyond the frontal profile of the turret, and the destabilizing yaw moments possibly occurred as a result of the fairings acting as lifting bodies. The flowfield surrounding the rotated fairings induced a pressure differential between the sides of the fairings. At small angles, this pressure differential was apparently responsible for the destabilizing yaw moments. This destabilizing phenomenon did not occur with the splitter plates, though.

If the turret were rotated beyond 5 deg, the fairings would begin to be visible to the freestream flow and more likely resemble bluff bodies and weathervane toward smaller sideslip angles. Safety concerns limited additional testing at larger sideslip angles because the fairing and splitter plate cantilevered mounting system was sensitive to lateral forces and twisting moments.

Effects of Testing Methods

Trip Strips

During the flow-visualization phase, tufts were placed almost exclusively along one side of the turret, fairings, and small splitter plate to facilitate viewing with still and high-speed video cameras.

Once the first fairing was attached to the turret, however, a significant amount of flow asymmetry was noted behind the turret. Tufts along the top of the fairing indicated a strong flow from the clean side of the fairing to the tufted side. In this configuration, the tufts introduced flowfield interference and caused early separation on the tufted side of the turret. However, flow stayed attached to the clean side of the turret for a longer distance and crossed over the centerline of the fairing.

A trip strip added to the clean side of the turret produced symmetric flow behind the turret for the remainder of the flow visualization study. A 1.3-cm- (0.5-in.-) wide strip of duct tape served as the trip strip, and it ran between the base and top of the turret. The leading edge of the strip was placed approximately 100 deg from the front of the turret to avoid increasing the profile area of the turret. Although the flow was already turbulent on reaching the trip strip (at higher tunnel velocities), the trip strip induced enough roughness to cause earlier separation from the otherwise smooth surface of the turret. The strip, therefore, matched the effective disturbances caused by the tufts on the tufted side of the turret.

When force data were taken in this study, the tufts were removed and an identical trip strip was placed opposite the existing trip strip. This configuration allowed the force data to correlate as closely as possible with the conditions shown in the tuft photos. The difference in drag (the main parameter measured) was small between the runs with trip strips installed or removed. The maximum change in drag was 4% at a velocity of approximately 44 m/s (144 ft/s), but the difference became negligible at higher velocities.

Cavity Opening

A 0.48-cm ($\frac{3}{16}$-in.) gap between the turret and surrounding cover plate was designed to allow for deflection of the turret and force measurement by the load-cell unit. Such a gap would not exist on the actual testbed aircraft, however, and the effects of having an open cavity beneath the turret model were investigated. To test the closed cavity, fiber tape was applied between the turret and cover plate on the underside of each. Enough slack was left in the tape to allow for deflections similar to those encountered in earlier runs. Modeling clay was placed in the remaining groove around the turret to create a surface flush with the ground plane. The clean turret was tested in this configuration by observing oil flows and recording force and pressure data.

At the highest tunnel speeds tested, the closed configuration drag was 3% less than that with the cavity open, and the difference was less at lower tunnel speeds. The stiffness of the tape and the modeling clay may have reduced the deflection of the turret and the measured drag. Also, there were no discernible flow differences noted in the oil distributions of the turret side flow between the open- and closed-cavity configurations. With no major flow differences or drag variations between the open- and closed-cavity configurations, the impact on the results of this study was minimal.

Error Analysis

The drag and pressure coefficients were analyzed to determine the level of uncertainty inherent in their final results. The drag coefficient only required knowledge of the drag force on the turret and the static pressure difference between atmospheric and the tunnel test section. Similarly, the pressure coefficient only needed two pressure readings: the pressure difference between the pressure taps and atmospheric pressure and the same test-section pressure measurement used for the drag coefficient. The uncertainty in each of these readings and the sensitivity of the various coefficients to each reading were determined to give the total estimated uncertainties shown in Fig. 16. Methods similar to those given by Holman and Gajda[10] were used.

High levels of uncertainty existed at lower tunnel speeds to an extent that the differences in drag between the clean-turret and both splitter plate configurations were suspect; however, at higher speeds, the uncertainty for each configuration was contained in narrower error bands. Neither fairing configuration showed an uncertainty that would change the results significantly in relationship to the clean turret. The load-cell unit had a 0.45 N (0.1-lbf) error.[4] At the lower

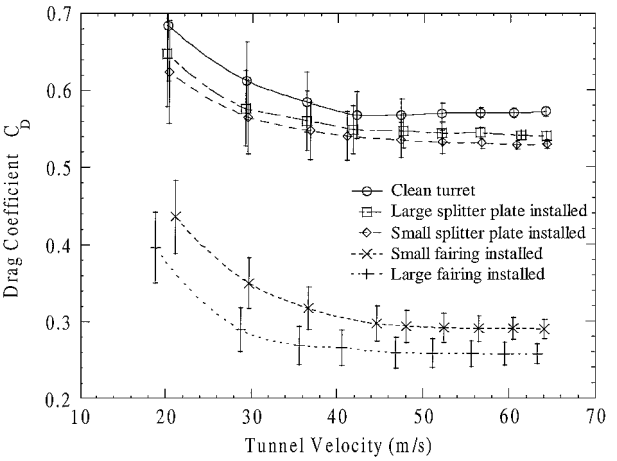

Fig. 16 Drag coefficient uncertainty.

tunnel velocities, drag forces were on the order of 4.45 N (1 lbf), and large errors resulted. The drag forces increased tenfold on the clean-turret and splitter plate configurations at higher velocities, resulting in a significant error reduction. When the fairings were attached, however, their success in reducing drag kept the measured drag levels near the range of low resolution for the load-cell unit. Unfortunately, the need to support the weight of the fairings and splitter plates in the cantilevered testing arrangement prohibited switching to weaker load cells with higher precision.

The results of the error analysis for the pressure coefficient data indicated that error bands for the pressure data were contained within the plot symbols for each data point. The automated pressure measurement system produced error levels of approximately 0.5% for each pressure tap.

Conclusions

This study characterized the flowfield around a turret model and determined the drag reduction with the addition of splitter plates and fairings to the turret that met the viewing requirements of the laser. The three-dimensional flow over the turret was driven by dominant top vortices that shed from the top of the turret and interacted with the vortices shed from the turret sides. This process formed a large low-pressure wake of vortices behind the turret that acted on the turret in the form of pressure drag. The splitter plates were not able to reduce the strength of the top vortices and only provided drag reductions of less than 10%.

The small fairing had a cross section that fit inside the separation region and did not change the separation point significantly from that of the unmodified turret. Nevertheless, this fairing reduced the baseline turret drag coefficient by 49%, but the flow quality near the turret was not significantly better than that of the clean-turret or splitter plate configurations. Also, the small fairing reduced the unobstructed field of regard by 30 deg over that of the splitter plate.

The large fairing was the most successful in reducing drag, resulting in a 55% drag coefficient reduction over the clean turret, but it reduced the unobstructed field of regard by an additional 30 deg over that of the small fairing. Flow also remained attached over most of the turret when the large fairing was attached, and the observed flow quality was much higher than any other configuration tested. Tufts, oil flow, and tuft-on-a-wire tests gave qualitative images of well-behaved flow in all areas, except a very small region near the turret/fairing junction. Clearly, the large fairing sacrificed laser field of regard in exchange for reduced separation and greater drag reduction.

References

[1]Hoerner, S. F., *Fluid-Dynamic Drag*, self-published, Midland Park, NJ, 1965.

[2]Mullane, R. M., "An Experimental Investigation of Methods of Suppressing the Unsteady Torque Exerted on the Upper Turning Mirror of an Aircraft Mounted Coelostat Turret," M.S. Thesis, AFIT/GAE/AE/75J-6, Dept.

of AeroMechanical Engineering, Air Force Inst. of Technology, Wright–Patterson AFB, OH, June 1975.

[3]Walterick, R. E., and Van Kuren, J. T., "Wind Tunnel Tests of Fairings for an On-Gimbal Telescope Turret," Air Force Flight Dynamics Lab., AFFDL-TM-75-177 FXM, Wright–Patterson AFB, OH, Nov. 1975.

[4]King, B. W., "Fluctuating Wind Forces Measured on a Bluff Body Extending from a Cavity," M.S. Thesis, AFIT/GAE/ENY/89D-19, Dept. of Aeronautics and Astronautics, Air Force Inst. of Technology, Wright–Patterson AFB, OH, Dec. 1989.

[5]Snyder, C. H., "Wind Tunnel Testing for Drag Reduction of an Aircraft Laser Turret," M.S. Thesis, AFIT/GAE/ENY/98J-02, Dept. of Aeronautics and Astronautics, Air Force Inst. of Technology, Wright–Patterson AFB, OH, June 1998.

[6]Rae, W. H., Jr., and Pope, A., *Low-Speed Wind Tunnel Testing*, 2nd ed., Wiley, New York, 1984, p. 371.

[7]Yang, W.-J., *Handbook of Flow Visualization*, Taylor and Francis, Ann Arbor, MI, 1989, p. 93.

[8]Belik, L., "The Secondary Flow About Circular Cylinders Mounted Normal to a Flat Plate," *The Aeronautical Quarterly*, Vol. 24, Feb. 1973, pp. 47–54.

[9]Shapiro, A. H., *The Dynamics and Thermodynamics of Compressible Fluid Flow*, Vol. 1, Ronald, New York, 1953, p. 410.

[10]Holman, J. P., and Gajda, W. J., Jr., *Experimental Methods for Engineers* 5th ed., McGraw–Hill, New York, 1989, p. 41.